Rheooscillations of a Bottlebrush Polymer Solution Due to Shear-Induced Phase Transitions between a Shear Molten State and a Line Hexatic Phase

Silke Rathgeber*

Polymer Physik, Max-Planck Institut für Polymerforschung, D-55128 Mainz, Germany

Hyung-il Lee and Krzysztof Matyjaszewski

Department of Chemistry, Carnegie Mellon University, Pittsburgh, Pennsylvania 15213

Emanuela Di Cola

European Synchrotron Radiation Facility, 38043 Grenoble Cedex, France

Received February 26, 2007; Revised Manuscript Received July 6, 2007

ABSTRACT: Time-resolved small-angle X-ray scattering (SAXS) experiments were carried out on concentrated solutions of bottlebrush polymers exposed to an external shear flow. We followed the rheological response of the sample online. If the experiment is performed in the strain-controlled mode, the rheological response of the bottlebrush polymer solution to the rotational shear shows oscillations with changes in viscosity of almost 2 orders of magnitude. The SAXS data reveal that this oscillatory response is due to a reentrant phase transition between a shear molten phase and a line hexatic phase. It is not due to shear-induced phase separation leading to shear band formation. The in-situ rheological SAXS measurements allow a detailed description of the structural changes occurring in the sample during structural buildup and breakdown.

Introduction

Compared to atomic and molecular crystals, elastic compliances of soft matter systems are much lower and structural relaxation times much longer. As a consequence, the coupling between an applied flow field and the structure of the system is strong. Thus, application of shear flow to soft matter systems can result in unusual behavior such as that steady shear can modify their structures and can induce new structures and textures that do not exist at rest.[1] The nature of the stationary phases can be summarized in a dynamic phase diagram as a function of the applied shear rate or stress. Dynamical transitions between the stationary states correspond to jumps between two branches of steady states. However, application of shear does not only result in stationary states. Transitions to oscillating states and chaotic-like behavior have been observed for various systems such as surfactant systems including wormlike micelles[3−14] and lamellar (onion) phases,[9−14] semiflexible colloidal rods,[15−17] and (liquid-crystalline) polymer solutions.[18−20] In most cases the rheochaotic behavior and the rheooscillation were accompanied by shear band formation, i.e., induced phase separation into banded structures in either the gradient or neutral direction. These bands can also undergo spatial and temporal fluctuations. The shear banding phenomenon is of mechanical, hydrodynamical origin. Rheochaos in these systems is discussed in terms of interface instabilities, fluctuations in wall slip, and structural fluctuations occurring in (one of) the bands. To our knowledge, there is only one study on a lamellar (onion) phase surfactant system showing that the chaotic-like rheological response is due to a structural transition of the whole sample from a disordered onion phase to an ordered onion phase.[9,10]

We report rheooscillation for concentrated solutions of shape-persistent macromolecules, so-called bottlebrush polymers exhibiting a rather persistent shape which is best described by a flexible cylinder with a smoothly radial decaying segment density profile.[24−26] The observed oscillating rheological response with changes in viscosity of almost 2 orders of magnitude is not due to shear band formation but is rather caused by a shear-induced phase transition between a line hexatic phase of aligned bottlebrush macromolecules and a shear molten state involving the whole sample.

Line hexatic phases have been proposed more than 20 years ago for nematic liquid crystals[27] and later for magnetic flux-line lattices in type II high-T_c superconductors[28] as a three-dimensional analogue of the two-dimensional hexatic phase, first predicted by Halperin and Nelson.[29] The characteristics of the line hexatic phase are long-range orientational and bond orientational order but short-range liquidlike positional order in the plane perpendicular to the axis of orientation. Experimental evidence has been found so far for polydisperse, chiral DNA molecules only.[30] There are also indications for a shear-induced line hexatic phase in oil-swollen surfactant tubes.[31]

Shear-induced melting has been observed for weak crystals formed by particles with ultrasoft interaction potential; i.e., the potential remains finite or diverges very slowly for zero separation.[32] Systems undergoing shear-induced melting include charged spheres with long-ranged Coulomb interaction[33,34] and copolymer micelles.[35] In a rough approximation shear melting can be described as the consequence of an instability originating from the subtle balance between disruptive forces between sliding layers and restoring elastic response within the layers. Within this approach the existence of a periodic restoring potential within the sliding layers is essential for the understanding of the melting transition. Shear-induced melting has also been observed for hexagonal, column phases of surfactant tubes swollen in oil.[31] The authors explain the melting transition in terms of proliferations of dislocations most likely longitudinal

* Corresponding author: Ph +49-6131-379-115; Fax +49-6131-379-100; e-mail s.rathgeber@mpip-mainz.mpg.de.

10.1021/ma070479g CCC: $37.00
Published on Web 09/15/2007

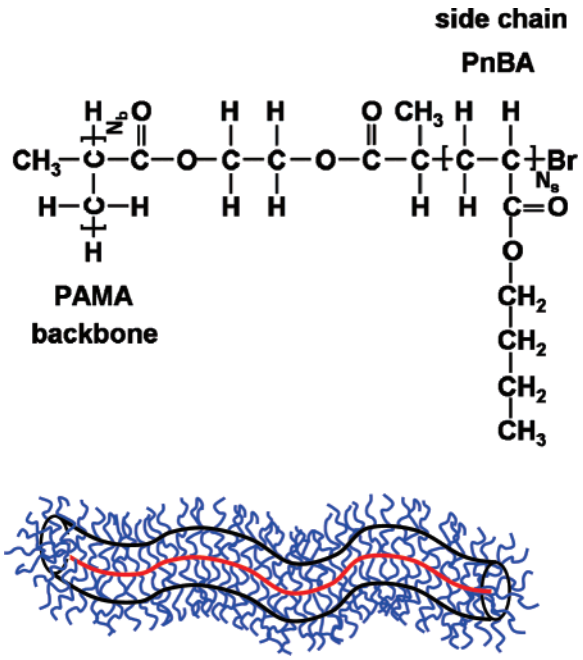

Figure 1. Chemical structure of the bottlebrush polymer with a PAMA backbone and PnBA side chains and a sketch visualizing its dense, cylindrical shape.

edge and screw dislocations which have low cost of energy in creation.

We followed the structural changes occurring in the sample during structural buildup and breakdown online by simultaneous performing rheological measurements and time-resolved experiments with small-angle X-ray scattering. The following discussion will give a detailed insight into the structural changes occurring during the shear-induced phase transition.

Experimental Section

Samples. The bottlebrush macromolecule under investigation was prepared via the grafting-from route. Figure 1 shows a schematic sketch of the structure. The sample consists of a hydroxyethyl methacrylic main chain prepared by atom transfer radical polymerization.[36,37] As described in earlier publications,[38,39] subsequent side chain functionalization with 2-(bromopropionyloxy)ethyl moiety yields initiation sites for controlled growth of poly(*n*-butyl acrylate) side chains. The macroinitiator was prepared by polymerizing trimethylsilyl-protected poly(2-hydroxyethyl methacrylate).[40,41] The number of monomers in the backbone and side chains are $N_s = 41$ and $N_b = 365$, respectively. The side chain initiation density was determined to be better than 95%. Details on the synthesis, characterization, and structure are given in previous publications where the sample was named B-365-41.[24,25] The shear experiments reported here were carried out under good-solvent conditions in toluene solutions with a polymer content of $\Phi_P = 20.0$ vol % at room temperature. A schematic of the chemical structure of the investigated bottlebrush macromolecule is given in Figure 1.

Rheology. Online rheological measurements were carried out with a Searle type RS300 rheometer of Thermo Haake GmbH, Germany, equipped with a cylindrical sample geometry having a gap width of $\Delta R = R_o - R_i = 1$ mm. The inner and outer cylinder with radii of $R_i = 10$ mm and $R_o = 11$ mm, respectively, were made from aluminum with a wall thickness of about 100 μm at the sample position. A constant shear rate of $\dot{\gamma} = 6\ s^{-1}$ was imposed onto the sample. The shear rate $\dot{\gamma}$ and shear strain τ were derived from the measured torque M and imposed angular frequency Ω using standard expressions $\Omega = \dot{\gamma}(R_o - R_i)/\bar{R} = 0.57$ rad s^{-1} with $\bar{R} = (R_o + R_i)/2$ and $\tau = M(2\pi R_i^2 L)^{-1}$, where $L = 40$ mm denotes the height of the inner cylinder. A detailed description of the setup is given in ref 42. As shown in Figure 2, two setups were used:

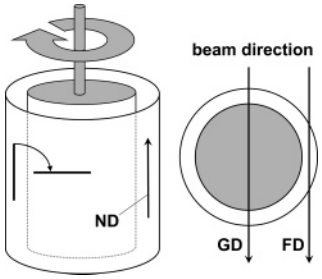

Figure 2. Schematic of the in-situ rheological SAXS experiment explaining the setup with the beam parallel to the flow direction (FD) and gradient direction (GD). The arrow in the cylinder gap marks the neutral direction (ND).

First, the tangential setup (FD) in which the beam traverses parallel to the flow direction probes structural changes occurring in the plane with normal vector in flow direction. Second, the radial setup (GD) in which the beam passes through the sample parallel to the gradient direction probes structures in the plane with normal vector in gradient direction.

SAXS. The small-angle X-ray experiments (SAXS) were carried out at the high brilliance beamline ID2 at the European Synchrotron Radiation facility in Grenoble, France. A detailed description of the in-situ rheological setup at ID2 is given in ref 42. The incident X-ray wave length was set to $\lambda = 0.10$ nm with a bandwidth of $\Delta\lambda/\lambda = 2 \times 10^{-4}$. With a detector-to-sample distance of $d = 3$ m an evaluable range of scattering vectors $0.11\ nm^{-1} \le q \le 2.97\ nm^{-1}$ was covered with the angle spread of $\Delta\theta = 25$ μrad. The q resolution of the experiment $\sigma_q = \sqrt{(q^2(\Delta\lambda/\lambda)^2 + (2\pi/\lambda)^2\Delta\theta^2)}/(8 \ln 2) \approx 6.8 \times 10^{-4}\ nm^{-1}$ is mainly determined by the angular spread. The contribution of the experimental resolution to the broadening of the peaks amounts to less than 0.15%. The size of the beam at the sample position in terms of the full width at half-maximum (FWHM) was 100 μm $\times$ 100 μm. Two-dimensional SAXS data were recorded using an image-intensified charge-coupled device camera and are corrected for background scattering following standard procedures described elsewhere.[43] Typical counting times for the flow (FD) and gradient direction (GD) were 0.5 s.

One-dimensional scattering data $I(q)$ are presented as a function of the norm of the scattering vector q (scattering angle θ) where averages are taken with a step width of $\Delta q = 0.0051\ nm^{-1}$ ($\Delta\theta = 8 \times 10^{-5}$°) over an opening angle of $\Delta\Phi = \pm 2$° around the respective peak positions. One-dimensional data $I(\Phi)$ are also plotted as a function of the azimuth angle Φ with a step width of $\Delta\Phi = 1$°, where cuts are taken through the respective peak positions ($\Delta q = 0.0051\ nm^{-1}$). The half-width at half-maximum (HWHM) of the peaks $\Delta\Phi_{HWHM}$ and Δq_{HWHM} are determined by fitting Lorentzian functions to the peaks in $I(\Phi)$ and $I(q)$, respectively.

The degree of orientation of the sample into the flow direction can be quantified in terms of the second rank order parameter P_2 which varies between 0 for a fully isotropic sample and 1 for a perfectly aligned sample. We followed the procedure described by Deutsch[21] which was i.a. successfully applied to cylindrical surfactant systems.[22,23] P_2 can be obtained from the $I(\Phi)$ cuts taken in GD through the first-order Bragg peaks

$$P_2 = 1 - \frac{3}{2N}\int_0^{\pi/2} d\Phi\, I(\Phi + \pi/2)\left[\sin^2\Phi + \cos^2\Phi \sin\Phi \ln\left(\frac{1+\sin\Phi}{\cos\Phi}\right)\right] \quad (1)$$

where the normalization constant is given by

$$N = \int_0^{\pi/2} d\Phi\, I(\Phi + \pi/2) \quad (2)$$

Results and Discussion

Shape and Lyotropic Behavior at Rest. SAXS experiments addressing the shape of the bottlebrush macromolecules under

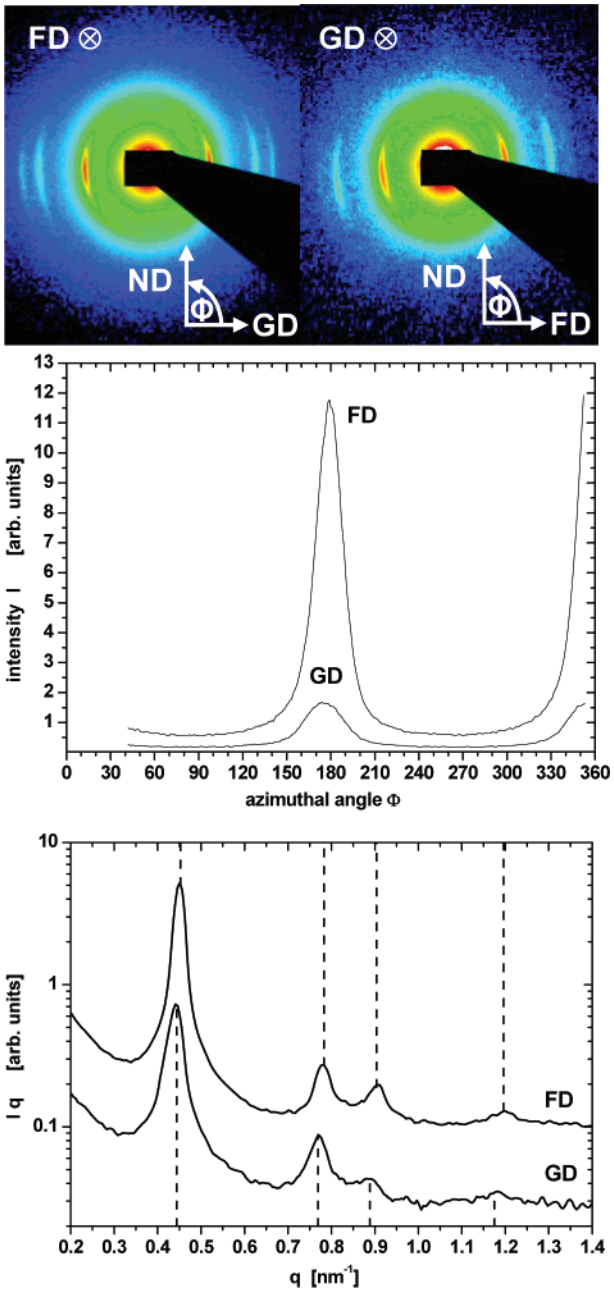

Figure 3. SAXS results obtained for the prealigned sample obtained for the FD and GD setup: two-dimensional SAXS pattern (top) and one-dimensional intensity data as a function of the azimuth angle Φ (middle) and as a function of the norm of the scattering vector q (bottom). The dashed lines mark the condition $1 \div \sqrt{3} \div 2 \div \sqrt{7}$.

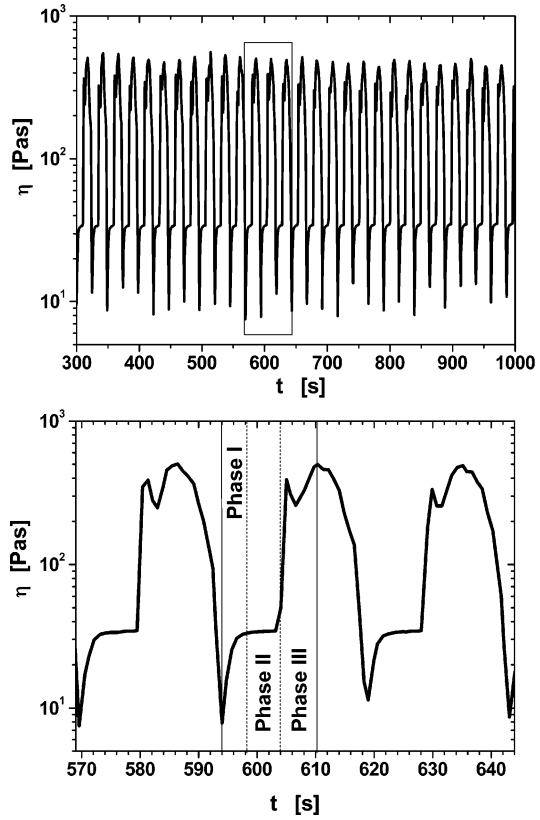

Figure 4. Rheological response of a concentrated bottlebrush polymer solution ($\Phi_P = 20.0$ vol %) prealigned in ND in the strain-controlled rheometer mode. The bottom part shows an enlargement of the boxed time window marked in the top part.

good-solvent conditions in dilute toluene solutions revealed that these polymers are rather shape persistent macromolecules and are best described as flexible cylinders built by few persistent segments of length, l_p, and a radial decaying density profile[24,25] (see sketch shown in Figure 1). The elongated, cylindrical shape of bottlebrush macromolecules is a consequence of sterical overcrowding of the side chains in the densely grafted brush and excluded volume interactions which lead to stretching of the backbone.

For the persistence length, l_p, we obtained $l_p = 35 \pm 2$ nm and for the ratio of the cylinder contour length L to l_p, $L/l_p = 3.2 \pm 0.2$. The aspect ratio in terms of the ratio of the persistence length to the diameter d of bottlebrush polymer determines the lyotropic behavior of the brushes. The diameter d can be estimated to be twice the cross-section radius of gyration $R_{CS,g} = 5.12 \pm 0.09$ nm of the bottlebrush polymers, yielding $l_p/d = 3.4 \pm 0.2$. The shear experiments reported here were carried out at room temperature under good-solvent conditions in toluene solutions with a polymer content of $\Phi_P = 20.0$ vol %. Previous SAXS experiments on concentrated solutions of the same bottlebrush macromolecule as studied here revealed lyotropic behavior.[25] At the polymer concentration prepared for the shear experiment the pronounced and narrow first-order peak on top of a broader peak indicates that the hexagonal phase with a correlation length ξ of the order of about $\xi = 200 \pm 5$ nm is in coexistence with the isotropic phase. The correlation length $\xi = \pi/\Delta q_{HWHM}$ was determined from the half-width at half-maximum (HWHM) Δq_{HWHM} of the first-order peak by a Lorentzian fit.

For flexible cylinders with hard-core interaction and ratios $l_p/d \leq 10$ comparable to that of the bottlebrush polymer under study, a transition from an isotropic phase via a biphasic region to a hexagonal phase is expected with increasing concentration.[43] For the bottlebrush polymer solution only the biphasic region is observed where isotropic and hexagonal phase coexist. There is no transition to a single hexagonal phase. Increasing the polymer content above the overlap concentration leads to a gradual melting of the structure, and finally only the isotropic phase is left at high polymer concentrations. Ordering phenomena in bottlebrush polymer solutions are a consequence of their rather shape persistent cylindrical structure, which in turn results from internal sterical overcrowding and excluded volume interactions. In contrast to flexible cylinders with hard-core interaction the bottlebrush polymers can interpenetrate each other. Above the overlap concentration, interpenetration leads to screening of the excluded volume interactions and to a

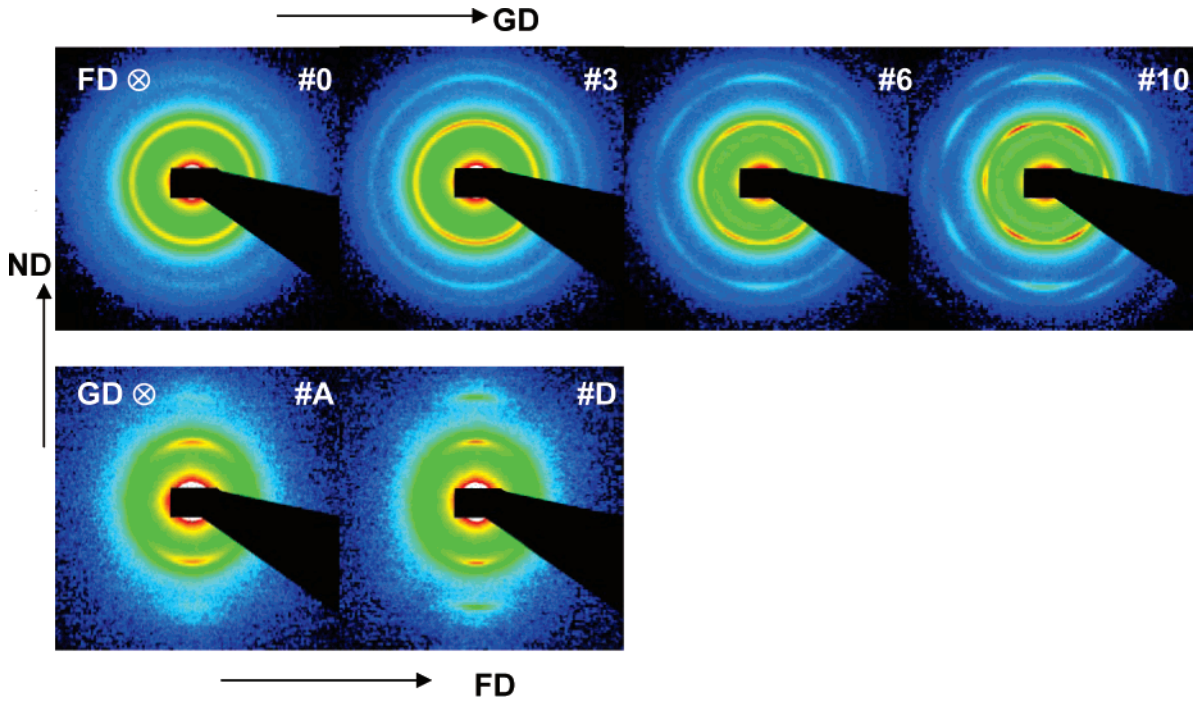

Figure 5. Representative two-dimensional SAXS pattern obtained for the sheared sample for the FD (top) and GD (bottom) setup. Labels (#"*x*") of the snap shots correspond to the labels used in Figures 8−10.

softening of the bottlebrush polymer structure. Thus, lyotropic behavior disappears at higher polymer contents.

Initial Condition before Shearing. To achieve a defined initial state of the sample before the constant rotational strain is applied, the sample is prealigned in the upright position parallel to the neutral direction (ND). Alignment was achieved by moving the rotor up and down. At maximum two cycles were required. The gap was not completely filled during the up and down movement, but the lower front side of the cylinder stayed in contact with the sample to avoid inclusion of air bubbles. The oscillating rheological response of the bottlebrush polymer solution was not affected by the perfectness of the prealignment. However, since partial prealignment occurs by moving the inner rotor to the measurement position, we were unable to realize a purely isotropic sample. The alignment of the sample seems to be persistent over longer time periods. Proof was taken for times up to about 1 h with no sign of structural relaxation. In Figure 3, the two-dimensional scattering pattern obtained in FD and GD are shown. From the Bragg peaks located at the azimuth angles of $\Phi = 0°$ and 180° we can conclude that the brushes are highly aligned with the longitudinal axis in ND. Here, Φ is measured from the GD for the FD setup and from the FD for the GD setup (see Figure 3). One-dimensional intensity data as a function of Φ and as a function of the norm of the scattering vector q are also shown in Figure 3. For a better visualizetion of the high q region the measured intensity is multiplied with the norm of the scattering vector. The q positions of the Bragg peaks can be assigned to a ratio of $1 \div \sqrt{3} \div 2 \div \sqrt{7}$ as expected for a multidomain, hexagonal structure of aligned rods where the symmetry axes of the domains rotate around the ND.

From the HWHM $\Delta\Phi_{HWHM}$ of the first-order Bragg peaks the degree of alignment of the longitudinal axes of the bottlebrush polymers can be quantified. Lorentzian fits yield $\Delta\Phi_{HWHM} = 10°$ and 15° for the FD and GD setup, respectively, showing that the bottlebrush polymers are highly aligned in ND. From the HWHM Δq_{HWHM} of the Bragg peaks in q the correlation length $\xi = \pi/\Delta q_{HWHM}$ of the structure can be estimated to be $\xi = 253 \pm 4$ nm and $\xi = 173 \pm 3$ nm in the planes perpendicular to the FD and GD, respectively. The experimental resolution contributes only to about 0.15% to the broadening of the Bragg peaks. From the peak location at $q^* = 0.450 \pm 0.005$ nm^{-1} (FD) and $q^* = 0.441 \pm 0.005$ nm^{-1} (GD) we obtain an interparticle spacing of $D = q^{*-1}4\pi/\sqrt{3} = 16.1 \pm 0.2$ nm (FD) and $D = 16.4 \pm 0.2$ nm (GD), respectively. Peak location and interparticle spacing obtained here are comparable to previous results on a nonaligned sample, where we obtained $q^* = 0.440 \pm 0.008$ nm^{-1} and $D = 16.5 \pm 0.3$ nm for a sample with a polymer concentration of $\Phi_P = 21$ vol %.[25] The spacing is larger than the diameter of the brushes in terms of twice the cross-sectional radius of gyration $2R_{CS,g} = 10.24 \pm 0.18$ nm. In Figure 8 of ref 25 the radial mass distribution perpendicular to the contour line of the bottlebrush polymer is presented. A comparison between (half of) the brush spacing and the radial mass distribution shows that the brushes significantly interpenetrate each other at the polymer content investigated here.

Sheared Sample. We followed the complex structural changes occurring in a perpendicular to the flow direction prealigned bottlebrush polymer solution in response to an applied constant strain and stress. In the stress-controlled rheometer mode the reorientation of the bottlebrush polymers into the flow direction is accompanied by a shear thinning process with a reduction in viscosity of 2 orders of magnitude. The reorientation process takes about 2 h and is accompanied by intermittent rheochaotical response due to complex structural changes occurring in the sample. However, this will be addressed by a future publication. Here we focus on the results obtained in the strain-controlled rheometer mode in which a shear-induced phase transition between a shear molten and a line-hexatic phase results in an oscillatory rheological response of the sample. In Figure 4, the viscosity oscillations of the bottlebrush solution in response to an imposed shear rate of $\dot{\gamma} = 6$ s^{-1} are shown. The viscosity changes almost 2 orders of magnitude with a periodicity of $\Delta t = 24.5 \pm 0.3$ s corresponding to a frequency of $\nu = (4.08 \pm 0.05) \times 10^{-2}$ Hz. The time for

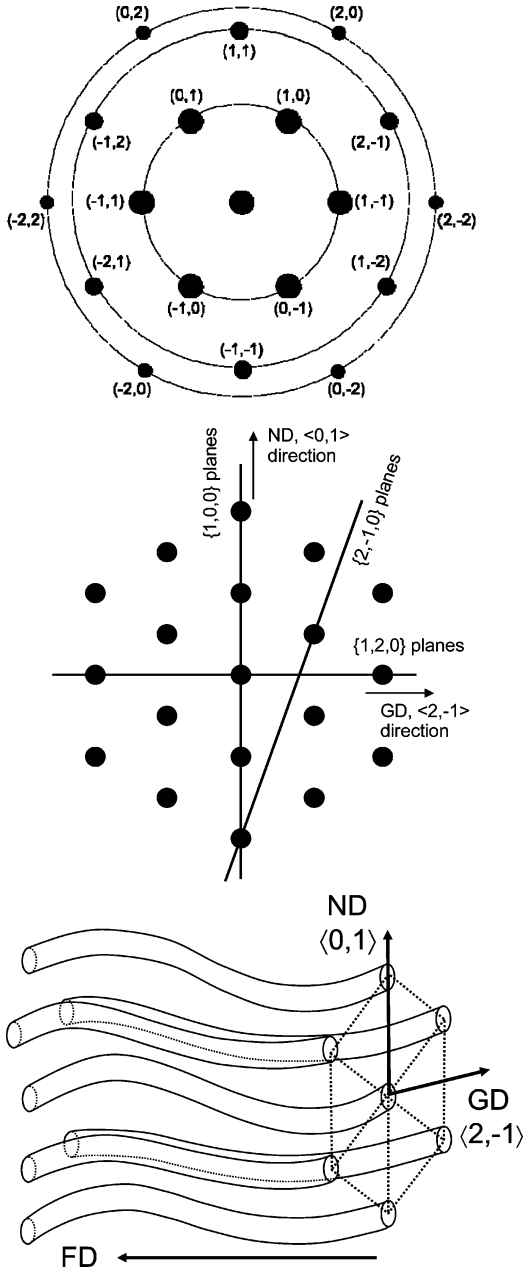

Figure 6. Nomenclature of the spots in the scattering pattern (top), corresponding structure in the plane perpendicular to the FD (middle), and schematics of the alignment of the bottlebrush polymers in respect to the ND, GD, and FD (bottom).

one full revolution of the inner cylinder is $T = 2\pi/\Omega = 11.0$ s where the angular frequency $\Omega = 0.57$ rad s^{-1} can be calculated from the geometry of the cylinder configuration as described in the Experimental Section. After a first sharp increase the viscosity settles to a short plateau before a second sharp increase sets in. This process takes about 10 s. After stagnating for about 5 s the viscosity continuously decreases within 10 s to its initial value. The oscillating rheological response seems not to be intermittent in nature. The signal maintains the same periodicity over longer time intervals. Proof was taken for times up to 45 min. We changed the shear rate in a limited range between $\dot{\gamma} = 2$ s^{-1} and $\dot{\gamma} = 10$ s^{-1} in increments of 2 s^{-1} and confirmed the asynchronous behavior between rotor period and torque oscillatory period. We obtained qualitatively similar results in terms of structural changes occurring in the sample and the oscillating rheological response for different shear rates.

To visualize the structural changes occurring in the sample during the increase of the viscosity, the two-dimensional scattering pattern is shown in Figure 5. The GD and FD setup probe structural changes occurring in the planes perpendicular to the GD and FD, respectively. The pictures to the left (#0 and #A) correspond to the low-viscosity state and those to the right (#10 and #D) to the high-viscosity state, as marked in Figure 4 by the solid lines. As can be seen from the GD pattern, the bottlebrush polymers are aligned in FD. The SAXS patterns taken in FD reveal that the low-viscosity state (FD, #0) corresponds to an isotropic state in the plane perpendicular to the flow direction. The first ring in the isotropic pattern corresponds to nearest-neighbor correlations. Higher order features are strongly suppressed. With time first a broad peak at an azimuth angle of $\Phi = 90°$ appears (FD, #3) before a pattern with hexagonal symmetry develops (FD, #6 and #10). In the high-viscosity state the scattering pattern with higher order features reveals a structure with hexagonal symmetry. As sketched in the upper part of Figure 6 and discussed in more detail in the following, the peak locations can be assigned to the pattern expected for a (two-dimensional) hexagonal closed-packed (hcp) structure. The hexagonal structure is aligned in respect to the ND, GD, and FD as depicted in the middle and bottom part of Figure 6. Peaks corresponding to directions with large components in GD [e.g., (± 1, ∓ 1), (± 2, ∓ 1), and (± 1, ∓ 2) spots] are less pronounced compared to those with large components in ND [e.g., (± 1, ± 1), (0, ± 1), and (± 1, 0) spots]. The velocity gradient across the gap of the cylinder configuration leads to a sliding of parallel planes with normal vectors in GD and weakens the ordering in this direction. Since the $\langle 0,1 \rangle$ directions are parallel to the ND, sliding planes are closed-packed planes. Because of the curvature of the cylinder and the final size of the beam in the FD setup, not only the plane perpendicular to the FD is probed. Planes tilted around the ND axis are also probed. This should leave spots in ND unaffected but can results in a weakening of spots with components in GD. However, the effect should increase when the beam position is shifted from the inner rotor along the gap to the outer wall. In Figure 7, the two-dimensional detector pattern of the hexagonal phase taken in FD are shown for three different beam positions along the gradient direction: (1) at the inner rotor, (2) in the gap center, and (3) at the outer wall. The corresponding $I(\Phi)$ cuts through the first-order Bragg peaks are also included. Surprisingly, there is no effect of the beam position on the intensity distribution in the peaks. Hence, we do not believe that the weakening of the spots with large ND components is due to nontangential contributions to the scattering pattern. For the FD and GD setup the nearest-neighbor correlation peaks appear at $q = 0.456 \pm 0.007$ nm^{-1}, corresponding to a spacing of the bottlebrush polymers of $D = 15.9 \pm 0.3$ nm. These values are comparable to the static results.

As mentioned above in the stress-controlled rheometer mode, the reorientation of the bottlebrush polymers into the flow direction is accompanied by a strong shear thinning process before finally a stable shear-molten state is reached. In the strain-controlled mode the rheometer enforces a defined shear velocity. In the crystalline state the viscosity is high and the rheometer has to impose a high force onto the sample to attain the predefined shear strain. It appears that the imposed high force leads to a melting of the ordered structure accompanied by a strong reduction in the sample viscosity. Thus, the rheometer can decrease the force necessary to keep the shear strain constant. The reduced force onto the bottlebrush polymer solution seems to provide the possibility for recrystallization.

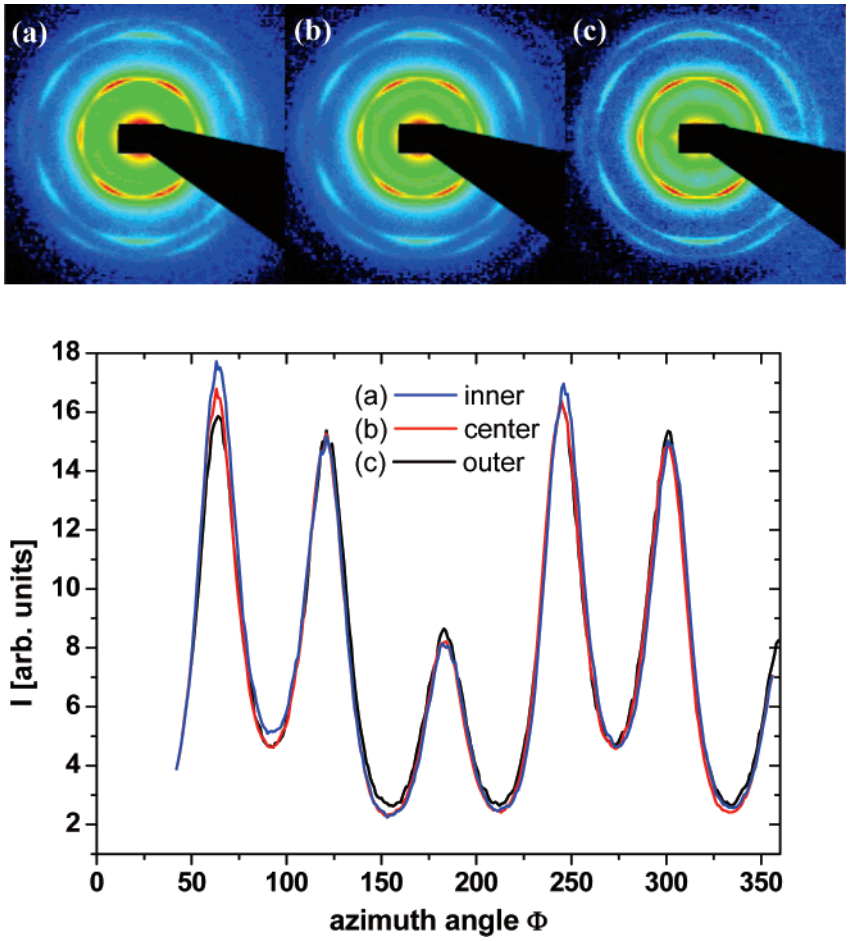

Figure 7. Representative two-dimensional SAXS pattern (top) obtained for the hexagonal structure of the sheared sample in the FD setup at different gap positions and corresponding $I(\Phi)$ cuts through the first-order Bragg-peaks (bottom): (a) at the inner rotor, (b) in the gap center, and (c) at the outer wall.

This mechanism would explain the periodic cycle of shear melting and recrystallization and the differences to the results obtained in the stress-controlled rheometer mode.

At equilibrium the bottlebrush polymers show lyotropic phase transitions from an isotropic to a biphasic region where a hexagonal and an isotropic phase coexist, followed by a reentrant melting transition. Shear flow strongly aligns rodlike entities and therefore affects the location of the phase boundaries. This can lead to shear-induced phase transitions, nonequilibrium phases, or pattern formation which have no equilibrium analogs.[15−17] Note that simple shear alignment would also occur for more flexible structures as long as the end-to-end distance relaxation time of the backbone is significantly longer as the inverse of the applied shear rate $\dot{\gamma}^{-1}$.

The goal of the following evaluation is to prove that these oscillations in viscosity are due to a transition between a shear molten state and a line hexatic phase. The SAXS results reveal that the structural changes occurring in the sample show the same repeatability of the cycling as does the rheological response. In the shear melting process the structural changes occur in reversal order and, thus, are not explicitly discussed in the following.

The line hexatic phase is characterized by long-range orientational and bond orientational order but short-range, liquidlike positional order perpendicular to the nematic axis of the polymers. Any cut through the sample perpendicular to the local director results in a collection of points at which the individual polymers pass through the cutting plane. Choosing any of these points as origin and going in any of the six well-defined directions of the hexagonal structure will bring you to another molecule. However, unlike in a crystal you do not know how far you must go. There is no twist in the positions of these points as the cut is shifted along the nematic axis of the molecules. The orientational and the bond orientational order can be quantified by evaluating the width of the first-order peaks in the $I(\Phi)$ cuts obtained for the GD and FD, respectively. The correlation length $\xi = \pi/\Delta q_{\mathrm{HWHM}}$ as a measure of the positional order of the developing structure can be quantified from the peak width Δq_{HWHM} in the $I(q)$ data. Figures 8−10 summarize the results obtained from the $I(q)$ and $I(\Phi)$ cuts. The upper part of Figure 8 shows representative one-dimensional intensity data for the FD setup as a function of q. For a better visualization of the high-q region the measured intensity is multiplied with the norm of the scattering vector. Cuts taken in ND (through the $(\pm1, \pm1)$ spots) together with averaged cuts through the $(\pm1, 0)$ and $(0, \pm1)$ spots are shown. The first peak corresponds to nearest-neighbor correlations. For the shear molten structure, higher order scattering features are suppressed which in the later stages gain strongly in intensity. The locations of the peaks are separated according to the ratio $1 \div \sqrt{3} \div 2 \div \sqrt{7}$ as expected for a hcp structure in the plane perpendicular to the FD.

Results for the correlation length ξ of the structure in the plane perpendicular to the FD obtained from the HWHM Δq_{HWHM} of the first-order Bragg peaks are presented in Figure 9. In the upper two parts of Figure 10 one-dimensional intensity cuts through the first-order Bragg peaks as a function of Φ are shown for the FD setup. From Figure 9 together with Figure

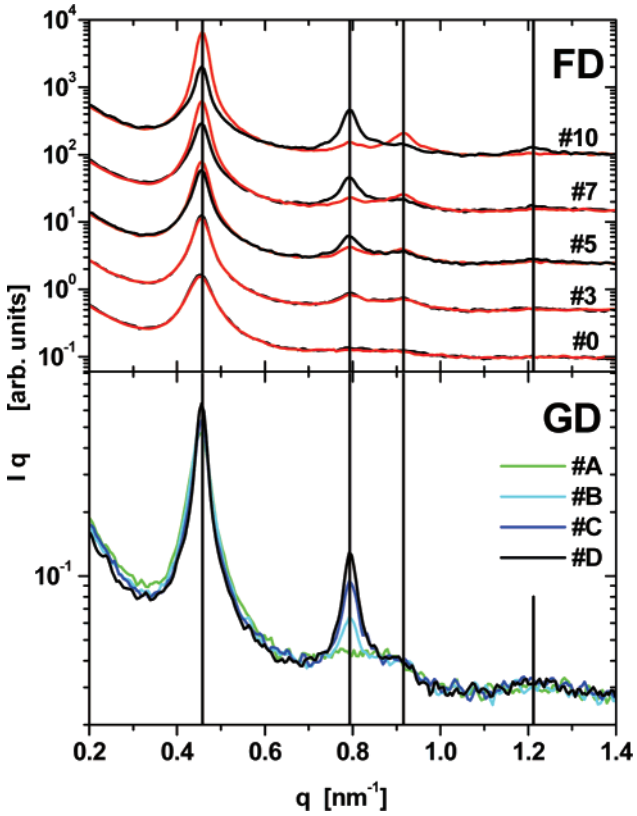

Figure 8. Representative one-dimensional SAXS results as a function of the norm of the scattering vector q. Top: FD setup with cuts taken through the ($\pm$1, $\pm$1) spots (ND, black curves) and averaged cuts through the ($\pm$1, 0) and (0, $\pm$ 1) spots (red curves) of the hexagonal pattern, respectively. Bottom: GD setup with cuts taken in ND. The solid lines mark the condition $1 \div \sqrt{3} \div 2 \div \sqrt{7}$. Labels (#"$x$") correspond to the labels used in Figures 5, 9, and 10.

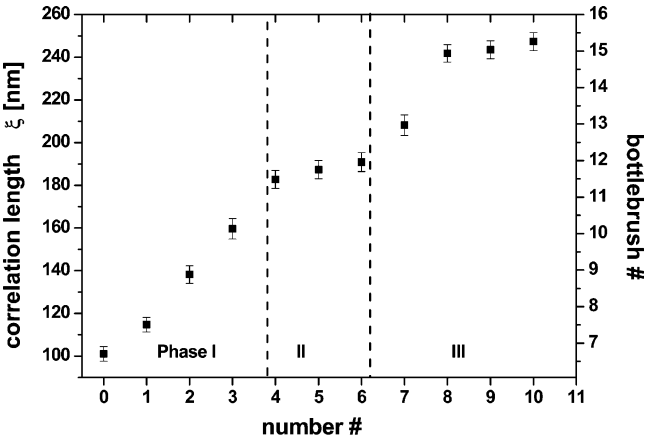

Figure 9. Correlation length ξ and number of bottlebrush polymers per correlation length of the hexagonal structure in the plane perpendicular to the FD. The x-axis gives the numbers (#"x") in correspondence to the labels used in Figures 5, 8, and 10.

10 three stages of the ordering process occurring in the plane with normal vector in FD can be distinguished. They are marked in Figure 9 and in the rheological response curve shown in Figure 4. (1) The spacing of the aligned cylinders becomes more defined in ND (broad peak at 90°). During the first stage of the structural buildup the correlation length ξ of the hcp structure increases from about 100 nm to about 180 nm; thus, correlations in positional order are lost over 3−5 nearest neighbors. The viscosity increases during this stage. (2) The order in GD starts to become more pronounced, and the typical hexagonal pattern appears which corresponds to a hexagonal structure with the

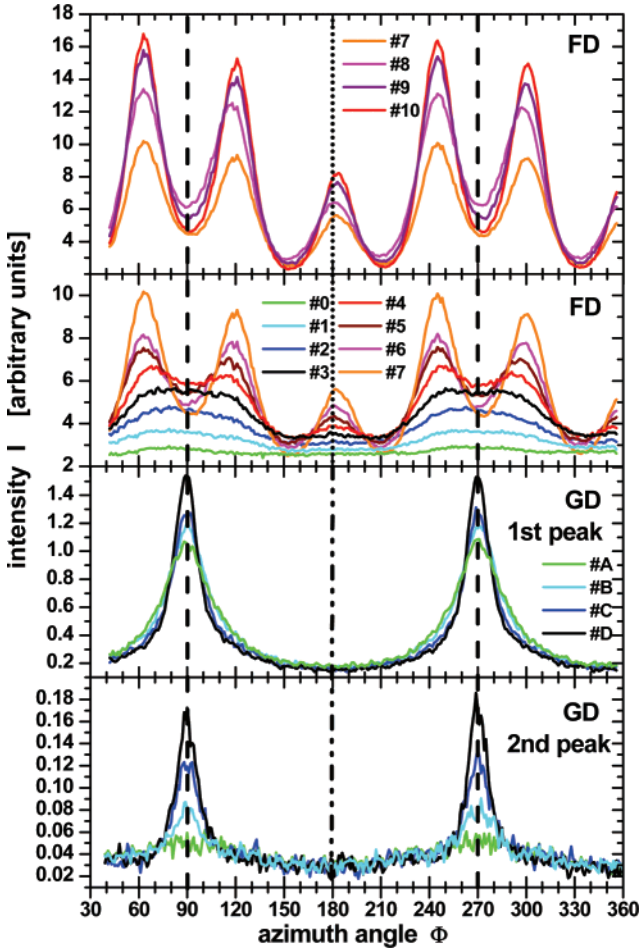

Figure 10. Representative one-dimensional intensity data as a function of the azimuth angle $I(\Phi)$. Top figures: temporal development of the first peak in the FD setup (#0−#10). Bottom figures: temporal development of the first and second peak in the GD setup (#A−#D). The dashed lines mark the ND. The dashed−dotted line and the dotted line mark the FD (bottom) and GD (top), respectively. Labels (#"x") correspond to the labels used in Figures 5, 8, and 9.

⟨0,1⟩ directions parallel to the ND. During this stage the correlation length stays almost constant as does the viscosity. (3) In the final stage the intensity of the peaks of the hexagonal pattern increases and their width decreases. The correlation length first increases rapidly from about 190 nm but then levels off around 250 nm. Thus, in the final state positional correlations extend over seven nearest neighbors and positional order is still small. This increase in domain size it not sufficient to explain the observed increase of peak intensities; therefore, an increase of the number of domains with the ⟨0,1⟩ directions parallel to the ND must also play a significant role. During this last stage of the structural buildup the viscosity first increases rapidly but later starts to stagnate. The HWHM $\Delta\Phi_{HWHM} = 12.4 \pm 0.3°$ of the first-order peaks of the final hexagonal structure is small, and thus we can conclude that the bond orientational order is high.

We now would like to focus on the structural changes occurring in the plane perpendicular to the GD. In the bottom part of Figure 8 representative q cuts through the Bragg peaks in ND are shown, and the two lower parts of Figure 10 present the corresponding Φ cuts through the nearest neighbor and the $\sqrt{3}$ peak. Aside from a small contribution of the ($\sqrt{3} \div 2$) peaks, in the shear molten state only the nearest-neighbor correlation peak shows up. For the later stages the nearest-neighbor correlation peak and the $\sqrt{3}$ peak gain in intensity.

The strong increase of the height of the $\sqrt{3}$ peak during structural buildup is in accordance with the interpretation that an increasing number of domains preferably orientate with the $\langle 0,1 \rangle$ directions parallel to the ND or analogous with the $\{1,2,0\}$ planes parallel to the GD direction (see Figure 6). The HWHM Δq_{HWHM} of the first-order Bragg peaks yields that positional order is lost over a length scale of $\xi = 122 \pm 1$ nm for the shear molten state (#A) and $\xi = 209 \pm 2$ nm for the state (#D) with the hexagonal structure in the plane perpendicular to the FD. These values correspond to about 3 and 6 nearest neighbors, respectively, and are in accordance with the results obtained for the FD. The orientational order measured in terms of $\Delta\Phi_{HWHM}$ of the first-order Bragg peaks (GD) enhances from $17.2 \pm 0.5°$ for the shear molten state (#A) to $8.5 \pm 0.2°$ for the final state (#D) with the hexagonal structure in the plane perpendicular to the FD. The orientational order can also be quantified by the order parameter P_2, which varies between 0 for a fully isotropic samples and 1 for an perfectly aligned sample (see eqs 1 and 2). We obtain $P_2 = 0.69$ for the shear molten state (#A) and $P_2 = 0.76$ for the final state (#D). Hence, it can be concluded that the bottlebrush polymers in particular in the latter case are strongly aligned in FD and orientational order is high. In conclusion, we proved the short-range positional order, long-range orientational order, and bond-orientational order which are the characteristic features of the line hexatic phase.

To check whether any indications for shear band formation can be found, we scanned the structure of the sample with different beam positions along the ND and GD. No indication for shear band formation was observed. Independent of the position in the gap the structural changes occurring in the sample show the same repeatability of the cycling in relation to the oscillatory rheological response. The shear molten state, the intermediate states, and the line hexatic phase can always be assigned to the same stages of the rheological response. In summary, we hence conclude that the rheooscillations observed here are due to a shear-induced reentrant phase transition between a shear molten state and a line hexatic phase involving the whole sample.

Because of the description of the bottlebrush polymers as flexible cylinders with radial decaying density profile, one can get the impression that an analogy to the semiflexible colloidal rods (fd viruses) investigated by Dhont and co-workers[15−17] can be drawn. The authors observed vorticity banding in steady shear flow both under controlled rate and stress conditions for samples with virus concentrations close to the isotropic−nematic phase transition in the absence of flow. However, one have to keep in mind that the fd virus with a diameter of $d = 7$ nm, a contour length of $L = 2.2$ μm, and a persistence length of $l_p = 880$ nm has a much more persistent shape with ratios $l_p/d = 312$ and $L/d = 125$. The bottlebrush polymer is a much more flexible entity $l_p/d = 3.4 \pm 0.2$ having a much smaller aspect ratio $L/d = 11 \pm 0.4$ compared to the fd virus. As a consequence, the bottlebrush polymer does not exhibit a lyotropic isotropic−nematic phase transition. In addition, the fd virus can be considered as a colloidal particle with hard-core interaction potential. The Gaussian-like radial segment density profile of the bottlebrush polymer results in an ultrasoft interaction potential, a prerequisite for the reentrant and shear-induced melting.

Conclusions

We performed in-situ rheological X-ray scattering experiments on a concentrated bottlebrush polymer solution under good-solvent conditions. In the strain-controlled mode we observed an oscillating rheological response of the sample with periodic changes in the viscosity of 2 orders of magnitude. Online scattering experiments allow a direct correlation between the rheological response and the structural changes occurring in the sample. The rheooscillations are a consequence of a shear-induced reentrant phase transition between a low-viscosity shear molten state and a line hexatic phase with high viscosity. The phase transition involves the whole sample; thus, the rheooscillations are not due to shear band formation as in most other cases where an oscillating or chaotic-like rheological response has been observed. To the best of our knowledge, there is only one more study on a lamellar (onion) phase surfactant system where the chaotic-like rheological response is due to a structural transition of the whole sample from a disordered onion phase to an ordered onion phase.[9,10] With the studies of Strey et al.[30] on polydisperse, chiral DNA molecules and Ramos and Molino[31] on oil-swollen surfactant tubes under shear, it is also to our knowledge the only experimental evidence for the appearance of a three-dimensional line hexatic phase.

Acknowledgment. We appreciate G. C. Berry for carefully reading the manuscript and for his helpful remarks. The financial support from NSF grant 06-09087 is greatly appreciated.

References and Notes

(1) Larson, R. G. *The Structure and Rheology of Complex Fluids*; Oxford University Press: New York, 1999.
(2) Cates, M. E.; Fieldings, S. M. *Adv. Phys.* **2006**, *55*, 799.
(3) Hu, Y. T.; Boltenhagen, P.; Matthys, E.; Pine, D. J. *J. Rheol.* **1998**, *42*, 1209.
(4) Bandyopadhyay, R.; Basappa, G.; Sood, A. K. *Phys. Rev. Lett.* **2000**, *84*, 2022.
(5) Bécu, L.; Manneville, S.; Colin, A. *Phys. Rev. Lett.* **2004**, *93*, 018301.
(6) López-González, M. R.; Holmes, W. M.; Callaghan, P. T.; Photinos, P. J. *Phys. Rev. Lett.* **2004**, *93*, 268302.
(7) Herle, V.; Fischer, P.; Windhab, E. J. *Langmuir* **2005**, *21*, 9051.
(8) Azzouzi, H.; Decruppe, J. P.; Lerouge, S.; Greffier, O. *Eur. Phys. J. E* **2005**, *17*, 507.
(9) Wunneberger, A. S.; Colin, A.; Leng, J.; Arnéodo, A.; Roux, D. *Phys. Rev. Lett.* **2001**, *86*, 1374.
(10) Salmon, J. B.; Colin, A.; Roux, D. *Phys. Rev. E* **2002**, *66*, 031505.
(11) Salmon, J. B.; Manneville, S.; Colin, A. *Phys. Rev. E* **2003**, *68*, 051504 & 051503.
(12) Manneville, S.; Salmon, J. B.; Colin, A. *Eur. Phys. J. E* **2004**, *13*, 197.
(13) Courbin, L.; Panizza, P.; Salmon, J.-B. *Phys. Rev. Lett.* **2004**, *92*, 018305.
(14) Ganapathy, R.; Sood, A. K. *Phys. Rev. Lett.* **2006**, *96*, 108301.
(15) Kang, K. G.; Lettinga, M. P.; Dogic, Z.; Dhont, J. K. G. *Phys. Rev. E* **2006**, *74*, 026307.
(16) Lettinga, M. P.; Dhont, J. K. G. *J. Phys.: Condens. Matter* **2004**, *16*, S3929.
(17) Dhont, J. K. G.; Lettinga, M. P.; Dogic, Z.; Lenstra, T. A. J.; Wang, H.; Rathgeber, S.; Carletto, P.; Willner, L.; Frielinghaus, H.; Lindner, P. *Faraday Discuss.* **2003**, *123*, 157.
(18) Quijada-Garrido, I.; Siebert, H.; Friedrich, C.; Schmidt, C. *Macromolecules* **2000**, *33*, 3844.
(19) Hilliou, L.; Vlassopoulos, D. *Ind. Eng. Chem. Res.* **2002**, *41*, 6246.
(20) Pujolle-Robic, C.; Noirez, L. *Phys. Rev. E* **2003**, *68*, 061706.
(21) Deutsch, M. *Phys. Rev. A* **1991**, *44*, 8264.
(22) Singh, M.; Agarwal, V.; De Kee, D.; McPherson, G.; John, V.; Bose, A. *Langmuir* **2004**, *20*, 5693.
(23) Roux, D. C.; Berret, J.-F.; Porte, G.; Peuvrel-Disdier, E.; Lindner, P. *Macromolecules* **1995**, *28*, 1681.
(24) Rathgeber, S.; Pakula, T.; Wilk, A.; Matyjaszewski, K.; Beers, K. L. *J. Chem. Phys.* **2005**, *122*, 124904.
(25) Rathgeber, S.; Pakula, T.; Wilk, A.; Matyjaszewski, K.; Lee, H.; Beers, K. L. *Polymer* **2006**, *47*, 7318.
(26) Zhang, B.; Gröhn, F.; Pedersen, J. S.; Fischer, K.; Schmidt, M. *Macromolecules* **2006**, *39*, 8440.
(27) Toner, J. *Phys. Rev. A* **1983**, *27*, 1157.

(28) Marchetti, M. C.; Nelson, D. R. *Phys. Rev. B* **1990**, *41*, 1910.
(29) Halperin, B. I.; Nelson, D. R. *Phys. Rev. Lett.* **1978**, *41*, 121.
(30) Strey, H. H.; Wang, J.; Podgornik, R.; Rupprecht, A.; Yu, L.; Parsegian, V. A.; Sirota, E. B. *Phys. Rev. Lett.* **2000**, *84*, 3105.
(31) Ramos, L.; Molino, F. *Phys. Rev. Lett.* **2004**, *92*, 018301.
(32) Likos, C. N. *Phys. Rep.* **2001**, *348*, 267.
(33) Ackerson, B. J.; Clark, N. A. *Phys. Rev. Lett.* **1981**, *46*, 123.
(34) Pusey, P. N. *Liquids, Freezing and the Glass Transition*; Elsevier: Amsterdam, 1991.
(35) Hamley, I. W. *J. Phys.: Condens. Matter* **2001**, *13*, R643 and references therein.
(36) Wang, J. S.; Matyjaszewski, K. *J. Am. Chem. Soc.* **1995**, *117*, 5614.
(37) Matyjaszewski, K.; Xia, J. *Chem. Rev.* **2001**, *101*, 2921.
(38) Börner, H.; Matyjaszewski, K. *Macromol. Symp.* **2002**, *177*, 1.
(39) Beers, K.; Gaynor, S.; Matyjaszewski, K.; Sheiko, S. S.; Möller, M. *Macromolecules* **1998**, *31*, 9413.
(40) Börner, H. G.; Duran, D.; Matyjaszewski, K.; da Silva, M.; Sheiko, S. S. *Macromolecules* **2002**, *35*, 3387.
(41) Matyjaszewski, K.; Ziegler, M. J.; Arehart, S. V.; Greszta, D.; Pakula, T. *J. Phys. Org. Chem.* **2000**, *13*, 775.
(42) Panine, P.; Gradzielski, M.; Narayanan, T. *Rev. Sci. Instrum.* **2003**, *74*, 2451.
(43) Narayanan, T.; Diat, O.; Boesecke, P. *Nucl. Instrum. Methods Phys. Res.* **2001**, *177*, 1005.
(44) van der Schoot, P. *J. Chem. Phys.* **1996**, *104*, 1130.

MA070479G